

Nematicity with a twist: rotational symmetry breaking in a moiré superlattice

Rafael M. Fernandes¹ and Jörn W. F. Venderbos^{2,3}

¹*School of Physics and Astronomy, University of Minnesota, Minneapolis, Minnesota 55455, USA*

²*Department of Physics, Drexel University, Philadelphia, PA 19104, USA*

³*Department of Materials Science & Engineering, Drexel University, Philadelphia, PA 19104, USA*

(Dated: November 27, 2019)

Motivated by recent reports of nematic order in twisted bilayer graphene (TBG), we investigate the impact of the triangular moiré superlattice degrees of freedom on nematicity. In TBG, the nematic order parameter is not Ising-like, as it is the case in tetragonal crystals, but has a 3-state Potts character related to the threefold rotational symmetry (C_{3z}) of the moiré superlattice. We find that even in the presence of static strain that explicitly breaks the C_{3z} symmetry, the system can still undergo a nematic-flop phase transition that spontaneously breaks in-plane twofold rotations. Moreover, elastic fluctuations, manifested as acoustic phonons, mediate a nemato-orbital coupling that ties the orientation of the nematic director to certain soft directions in momentum space, rendering the Potts-nematic transition mean-field and first-order. In contrast to the case of rigid crystals, the Fermi-surface hot-spots associated with these soft directions are maximally coupled to the low-energy nematic fluctuations in the case of the moiré superlattice.

Introduction. Twisted bilayer graphene (TBG) offers a tantalizing platform to explore the combined role of effects typically found separately in strongly correlated materials, topological matter, and two-dimensional systems. For “magic” twist angles, the phase diagram of TBG displays a rich landscape, showcasing superconductivity, correlated insulating behavior, ferromagnetism, and anomalous quantum Hall effect [1–6]. Similar phases are also realized in other twisted compounds [7–11]. It is believed that this rich physics arises due to the emergence of isolated—and possibly topologically non-trivial—nearly-flat bands in the Brillouin zone associated with the moiré superlattice [12–30]. This triangular superlattice, with lattice constant of the order of 10 nm, is formed by the AA stacking regions, where two carbon atoms from the two graphene layers sit atop each other [Fig. S1(a)]. The very small bandwidth, of about 10 meV, combined with an estimated Coulomb energy of tens of meV, indicate that correlations play a crucial role in TBG [31]. Indeed, correlated insulating phases are observed at nearly all commensurate fillings of the moiré unit cell [2–4], which can host eight electrons.

Scanning tunneling microscopy [32–34] and transport measurements [35] have recently reported evidence that the three-fold rotational symmetry of the moiré superlattice, denoted by C_{3z} , is broken in different regions of the TBG phase diagram. Moreover, spontaneous C_{3z} symmetry-breaking has been invoked to explain the observed Landau level degeneracy at charge neutrality [36, 37]. These observations are suggestive of an electronic nematic phase, i.e. a correlation-driven lowering of the point group symmetry of a crystal [38, 39]. Theoretically, a C_{3z} symmetry-breaking phase has been predicted by some models [40–44]. Experimentally, however, it is a difficult task to distinguish spontaneous nematic order from an explicit broken symmetry caused by strain,

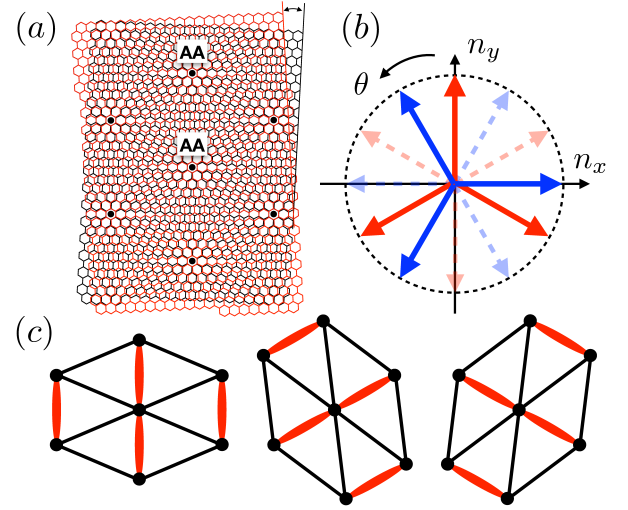


FIG. 1. (a) Triangular moiré superlattice of TBG, formed by the AA stacking regions (black dots). (b) Allowed directions of the nematic director $\hat{\mathbf{n}} = (\cos\theta, \sin\theta)$; blue (red) corresponds to $\gamma < 0$ ($\gamma > 0$) in the action Eq. (1). Note that \mathbf{n} and $-\mathbf{n}$ (dashed arrows) are identified. (c) moiré superlattice distortion in the presence of the three symmetry-related Potts-nematic orders, depicted as a pattern of inequivalent bonds.

whose presence is ubiquitous in TBG [34, 45–47].

In this paper, we investigate the interplay between electronic nematic order and static and fluctuating strain in moiré superlattices, applying our results to TBG. Nematic order in hexagonal (super)lattices, such as TBG, is fundamentally different from its more well-known counterpart in tetragonal systems, such as pnictides and cuprates [38, 48]. Whereas the latter is described by an Ising order parameter, the former is described by a two-component order parameter in the 3-state Potts-model class. As a result, the impact of lattice degrees of freedom

is very different. While static strain completely smears the nematic transition in tetragonal lattices, it allows the moiré superlattice to still undergo an Ising-like nematic-flop transition, in which in-plane twofold rotational symmetries are spontaneously broken. Finite-momentum strain fluctuations, manifested as acoustic phonons, mediate a non-analytic nemato-orbital coupling in the moiré superlattice. The latter makes certain directions in momentum space – which are tied to the nematic director’s orientation – softer than others across the nematic transition. This renders the 3-state Potts-nematic transition mean-field and first-order, and also constrains the electronic states that can exchange low-energy nematic fluctuations to a discrete set of Fermi surface hot-spots. Because the moiré superlattice is not a rigid crystal [49, 50], the nematic form factor is maximum at these hot-spots. This contrasts with rigid lattices, where the form factor vanishes at the hot spots, effectively decoupling the electronic system from low-energy nematic fluctuations. Thus, the maximum coupling between hot spots and nematic fluctuations makes moiré superlattices promising systems to elucidate the impact of nematicity on electronic properties.

Potts-nematic order. Nematic order is described by a traceless symmetric tensor, which in two dimensions has two independent components Φ_1 and Φ_2 corresponding to the charge quadrupole moments with $d_{x^2-y^2}$ and d_{xy} symmetries, respectively. In systems with tetragonal symmetry, these two d -waves have distinct symmetry and must thus be treated as two independent Ising order parameters. This is markedly different in hexagonal systems, such as TBG with point group D_6 [51]: the two nematic components belong to a single irreducible representation of D_6 and transform as partners under its symmetries, defining a two-component order parameter $\Phi = (\Phi_1, \Phi_2)$. It is natural to parametrize it as $\Phi = \Phi(\cos 2\theta, \sin 2\theta)$, where the angle θ can be identified with the orientation of the nematic director $\hat{\mathbf{n}} = (\cos \theta, \sin \theta)$ (see Fig. S1); note that $\Phi(\theta) = \Phi(\theta + \pi)$, as expected.

Although this parametrization might suggest that Φ is an XY order parameter, the lattice symmetries of TBG introduce crystal anisotropy effects that pin the nematic director to a discrete set of high-symmetry directions. Indeed, the Landau-type action $S_{\text{nem}}[\Phi]$ is (see also [40, 52–54]):

$$S_{\text{nem}}[\Phi] = S_0[\Phi] + \frac{\gamma}{6} \int_x (\Phi_+^3 + \Phi_-^3), \quad (1)$$

where $x = (\mathbf{r}, \tau)$ denotes spatial coordinate \mathbf{r} and imaginary time τ , and $\Phi_{\pm} \equiv \Phi_1 \pm i\Phi_2$. The first term, $S_0[\Phi] = \frac{1}{2}r_{\Phi}|\Phi|^2 + \frac{1}{4}u_{\Phi}|\Phi|^4$, is a standard Φ^4 -action with U(1) symmetry. The cubic term reflects the crystalline anisotropy of the hexagonal lattice, and is expressed as $\frac{1}{3}\gamma\Phi^3 \cos 6\theta$, which is minimized by $\theta = 2n\pi/6$ for $\gamma < 0$, and $\theta = (2n+1)\pi/6$ for $\gamma > 0$. These solutions correspond to sets of threefold degenerate nematic directors,

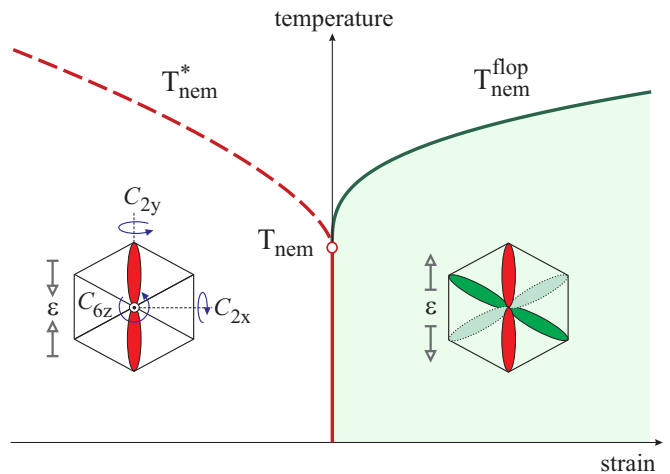


FIG. 2. Schematic temperature *vs* strain phase diagram with strain applied along the y -axis ($\alpha = \pi/2$) and $\lambda < 0$, $\gamma > 0$. For compressive strain ($\varepsilon < 0$), because the director is fixed at $\theta_0 = \pi/2$, which is a minimum of the cubic term, no phase transition occurs, and only a crossover temperature T_{nem}^* survives. For tensile strain ($\varepsilon > 0$), the director is at $\theta_0 = 0$, which is a maximum of the cubic term, for $T > T_{\text{nem}}^{\text{flop}}$, and at $\pm\theta_0$ for $T < T_{\text{nem}}^{\text{flop}}$. Thus, $T_{\text{nem}}^{\text{flop}}$ marks an Ising-like nematic-flop transition in which the twofold rotational symmetries C_{2x} and C_{2y} are spontaneously broken (dark/light green bonds). The sixfold rotation C_{6z} is explicitly broken to C_{2z} everywhere for $\varepsilon \neq 0$ (red bonds).

as shown in Fig. S1(b) [recall that angles differing by π (dashed arrows) must be identified], and manifested as bond orders in real space [Fig. S1(c)]. Eq. (1) is the continuum version of the 3-state Potts-model, with the \mathbb{Z}_3 symmetry identified with the out-of-plane threefold rotation C_{3z} . Below the nematic transition temperature T_{nem} , the sixfold rotation symmetry C_{6z} is lowered to a twofold symmetry C_{2z} , while the perpendicular twofold rotations C_{2x} and C_{2y} (or their symmetry-related equivalents) are preserved (see inset of Fig. S2). Despite the presence of a cubic term in (1), the 3-state Potts transition is continuous in two dimensions [55].

Static strain. As shown in Fig. S1(c), a lattice distortion is triggered by nematic order. We include the elastic degrees of freedom via the strain tensor $\varepsilon_{ij} \equiv \frac{1}{2}(\partial_i u_j + \partial_j u_i)$ and the rotation tensor $\omega_{ij} \equiv \frac{1}{2}(\partial_i u_j - \partial_j u_i)$, where \mathbf{u} is the moiré-superlattice displacement vector. The elasto-nematic action is given by $S_{\text{el-nem}}[\Phi, \hat{\varepsilon}, \hat{\omega}] = S_{\text{el}}[\hat{\varepsilon}, \hat{\omega}] + S'[\Phi, \hat{\varepsilon}]$, where $S_{\text{el}}[\hat{\varepsilon}, \hat{\omega}]$ is the elastic free energy and:

$$S'[\Phi, \hat{\varepsilon}] = -\lambda \int_x [(\varepsilon_{xx} - \varepsilon_{yy}) \Phi_1 + 2\varepsilon_{xy} \Phi_2]. \quad (2)$$

with coupling constant λ . Consider first the effect of static strain. For compressive (tensile) uniaxial strain $\varepsilon < 0$ ($\varepsilon > 0$) applied parallel to an arbitrary direction $\hat{\mathbf{d}}$, the action above becomes $S' = -\lambda \int_x \varepsilon \Phi \cos(2\alpha - 2\theta)$, where $\cos \alpha = \hat{\mathbf{d}} \cdot \hat{\mathbf{x}}$. At high temperatures $T \gg T_{\text{nem}}$,

where T_{nem} is the transition of the unstrained system, we can approximate $S_{\text{nem}} \approx \frac{1}{2} \int_x \chi_{\text{nem}}^{-1} \Phi^2$. Thus, strain not only triggers a finite nematic order parameter $\Phi \propto \chi_{\text{nem}} |\varepsilon|$, but it also pins the nematic director parallel or perpendicular to the strain direction, i.e. $\theta_0 = \alpha$ or $\theta_0 = \alpha + \pi/2$, depending on whether $\lambda\varepsilon > 0$ or $\lambda\varepsilon < 0$, respectively. To understand what happens as temperature is lowered, we consider $T \ll T_{\text{nem}}$ and set $|\Phi| = \Phi_0$ as approximately constant. Expanding around the high-temperature director, $\theta = \theta_0 + \delta\theta$, gives:

$$S_{\text{nem}} + S' = \int_x \left[a_{\theta_0} (\delta\theta) + b_{\theta_0} (\delta\theta)^2 \right] \quad (3)$$

with coefficients $a_{\theta_0} = -2\gamma\Phi_0^3 \sin 6\theta_0$ and $b_{\theta_0} = 2\Phi_0 (|\lambda\varepsilon| - 3\gamma\Phi_0^2 \cos 6\theta_0)$. If α (and consequently θ_0) does not coincide with the minima/maxima of the cubic term, i.e. $\alpha \neq n\pi/6$, then $a_{\theta_0} \neq 0$. As a result, θ evolves continuously from its high-temperature value θ_0 , and no phase transition occurs. However, when strain is applied along a high-symmetry direction ($\alpha = n\pi/6$), $a_{\theta_0} = 0$ and the twofold rotations C_{2x} and C_{2y} are preserved. These symmetries can nevertheless be spontaneously broken if $b_{\theta_0} < 0$. This can only happen if θ_0 coincides with the maxima, but not the minima, of the cubic term – in other words, if the strain term S' is minimized by a director that is maximally penalized by the cubic term of S_{nem} . In this case, once Φ_0 reaches the critical value $\bar{\Phi}_0 = \sqrt{\left| \frac{\lambda\varepsilon}{3\gamma} \right|}$, usually at a temperature $T_{\text{nem}}^{\text{flop}} > T_{\text{nem}}$, the minimum changes from θ_0 to $\theta_0 \pm \bar{\theta}_0$, with $\bar{\theta}_0 = \frac{1}{2} \arccos \left(\frac{1}{2} \sqrt{1 + \frac{3\bar{\Phi}_0^2}{\Phi_0^2}} \right)$, resulting in an Ising-like transition that spontaneously breaks the C_{2x} and C_{2y} symmetries. Due to its resemblance to the spin-flop transition, we dub the reorientation of the nematic director under an external field a nematic-flop transition. Thus, as illustrated in the phase diagram of Fig. S2, a nematic-driven phase transition can still occur in a strained triangular lattice [55, 56], in contrast to the case of a strained tetragonal lattice, where only a crossover exists. Therefore, the observation of a spontaneous C_{2x}/C_{2y} symmetry-breaking in strained TBG would provide direct evidence for long-range nematic order.

Fluctuating strain. Besides static strain, finite-momentum elastic fluctuations strongly impact the nematic transition [57–59]. Generally, for a system with D_6 symmetry, diagonalization of the harmonic elastic action $S_{\text{el}}[\hat{\varepsilon}, \hat{\omega}]$ leads to two acoustic phonon modes, a transverse (T) and a longitudinal (L) one with sound velocities $v_{L,T}$:

$$S_{\text{el}} = \frac{1}{2} \sum_{\mu=L,T} \int_q \tilde{u}_{q,\mu} (\omega_n^2 + v_\mu^2 \mathbf{q}^2) \tilde{u}_{-q,\mu}, \quad (4)$$

where $q = (\mathbf{q}, \omega_n)$, with ω_n the (bosonic) Matsubara frequency. The displacement field $\mathbf{u} = \sum_\mu \tilde{u}_\mu \hat{\mathbf{e}}_\mu$

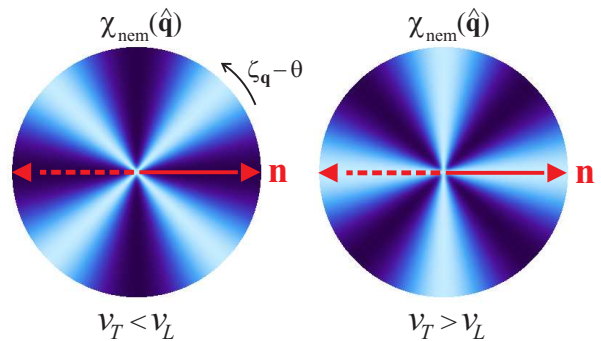


FIG. 3. Momentum-directional dependence of the nematic susceptibility $\chi_{\text{nem}}(q \rightarrow 0, \hat{\mathbf{q}})$ caused by the nemato-orbital coupling, with $\hat{\mathbf{q}} = (\cos \zeta_{\mathbf{q}}, \sin \zeta_{\mathbf{q}})$. Light blue (dark blue) denotes softer (harder) directions, corresponding to higher (lower) susceptibility. While for a rigid crystal, $v_T < v_L$, the soft direction is rotated by $\pm\pi/4$ with respect to the nematic director \mathbf{n} (red arrow), for TBG, $v_T > v_L$, the rotation is 0, $\pi/2$. Note that the director can point in any of the directions θ of Fig. S1(b).

has been decomposed into its longitudinal and transverse components \tilde{u}_μ with $\hat{\mathbf{e}}_L = (\cos \zeta_{\mathbf{q}}, \sin \zeta_{\mathbf{q}})$ and $\hat{\mathbf{e}}_T = (-\sin \zeta_{\mathbf{q}}, \cos \zeta_{\mathbf{q}})$ and $\zeta_{\mathbf{q}} = \arctan(q_y/q_x)$. According to Refs. [49, 50], for the dominant acoustic phonons that act on the moiré superlattice scale, \mathbf{u} corresponds to the relative displacement of the two graphene sheets. These and other phonon modes have been proposed to be linked to superconductivity in TBG [25, 60–62]. Integrating out the acoustic phonons leads to an additional contribution to the nematic action, $\delta S_{\text{nem}} = -\frac{1}{2} \sum_{ij} \int_q \Phi_{i,q} \hat{\Pi}_{ij}(q) \Phi_{j,-q}$. In the static limit, $\omega_n = 0$, we find:

$$\hat{\Pi} = \frac{\lambda^2}{v_T^2} \left[\hat{\mathbb{I}} - \eta \hat{\mathbb{P}} \right], \quad \hat{\mathbb{P}} = \begin{pmatrix} \cos^2 2\zeta_{\mathbf{q}} & \frac{1}{2} \sin 4\zeta_{\mathbf{q}} \\ \frac{1}{2} \sin 4\zeta_{\mathbf{q}} & \sin^2 2\zeta_{\mathbf{q}} \end{pmatrix} \quad (5)$$

where $\hat{\mathbb{I}}$ is the identity matrix and $\eta \equiv 1 - v_T^2/v_L^2$. The first term of $\hat{\Pi}$ gives an overall enhancement of T_{nem} . The second term couples the two nematic components Φ_1 and Φ_2 in a way that depends on the direction, but not on the magnitude of \mathbf{q} . Such a non-analytic term typically appears when order parameters couple linearly to an elastic mode [63], and was previously studied for Ising-nematic order in tetragonal lattices [57, 58]. Here, it is manifested as a nemato-orbital coupling:

$$S_{\text{nem}}^{\text{(eff)}}[\Phi] = S_0[\Phi] + \frac{\gamma}{6} \int_x (\Phi_+^3 + \Phi_-^3) + \frac{\lambda^2}{v_T^2} \left[- \int_x \Phi^2 + \eta \int_q (\Phi \cdot \hat{\mathbf{D}})^2 \right] \quad (6)$$

where $\hat{\mathbf{D}} = (\cos 2\zeta_{\mathbf{q}}, \sin 2\zeta_{\mathbf{q}}) = (\hat{q}_x^2 - \hat{q}_y^2, 2\hat{q}_x \hat{q}_y)$ is the momentum-space (i.e. orbital) quadrupolar form-factor. Recasting the nemato-orbital coupling term as $\Phi^2 \cos^2(2\theta - 2\zeta_{\mathbf{q}})$, we see that it makes only certain directions of momentum space to become soft, i.e. the

static nematic susceptibility $\chi_{\text{nem}}(q \rightarrow 0, \hat{\mathbf{q}})$ is largest near T_{nem} only along special directions $\hat{\mathbf{q}}$ (see also [58]). While the cubic term in Eq. (6) forces the director $\hat{\mathbf{n}}$ to point along one of three directions [Fig. S1(b)], the nemato-orbital coupling makes only two momentum-space directions $\zeta_{\mathbf{q}}$ soft, namely, the ones that make a relative angle of 0 and $\frac{\pi}{2}$ (for $\eta < 0$) or $\pm\frac{\pi}{4}$ (for $\eta > 0$) with respect to $\hat{\mathbf{n}}$ [see Fig. S3]. The reduction of the soft-direction phase-space from continuous to discrete is known to effectively enhance the dimensionality of the Φ^4 -action $S_0[\Phi]$ from d to $d+1$ [64]. Thus, one expects that the nematic transition in the moiré superlattice will be the same as a three-dimensional 3-state Potts-model transition, which is mean-field and first-order [55].

Electronic degrees of freedom. If the first-order character of the nematic transition discussed above is weak, nematic fluctuations are still expected to impact the electronic degrees of freedom. For a single-band system with fermionic operator $c_{\mathbf{k}}$, the electronic-nematic coupling is $S_{\text{elec}} = \int_{\mathbf{k}, \mathbf{q}} g(\mathbf{k}) \Phi_{\mathbf{q}} c_{\mathbf{k}-\mathbf{q}/2}^\dagger c_{\mathbf{k}+\mathbf{q}/2}$, with form factor $g(\mathbf{k}) = g_0 \cos(2\theta - 2\theta_{\mathbf{k}})$, where g_0 is a constant and $\theta_{\mathbf{k}} = \arctan(k_y/k_x)$. The electronic states that exchange low-energy nematic fluctuations are at the Fermi surface and separated by the small momentum \mathbf{q} of the nematic mode. Since the nematic fluctuations are the softest (albeit non-diverging) along the special directions $\hat{\mathbf{q}}^{(0)} = (\cos \zeta_{\mathbf{q}}^{(0)}, \sin \zeta_{\mathbf{q}}^{(0)})$ discussed above, the relevant pairs of fermions are located around the ‘‘hot spots’’ \mathbf{k}_{hs} where the Fermi surface’s tangent is parallel to $\hat{\mathbf{q}}^{(0)}$, i.e. $\hat{\mathbf{q}}^{(0)} \cdot \nabla \zeta_{\mathbf{k}_{\text{hs}}} = 0$. The issue is how strong these fermions are coupled to the nematic fluctuations, i.e. what is the magnitude of $g(\mathbf{k}_{\text{hs}})$. For a circular Fermi surface, the hot spots are located at $\theta_{\mathbf{k}_{\text{hs}}} = \zeta_{\mathbf{q}}^{(0)} + \frac{\pi}{2}$, and thus $g(\mathbf{k}_{\text{hs}}) = -g_0 \cos(2\theta - 2\zeta_{\mathbf{q}}^{(0)})$. As we saw above, if $\eta > 0$, the soft directions are $\zeta_{\mathbf{q}}^{(0)} = \theta \pm \pi/4$, yielding $g(\mathbf{k}_{\text{hs}}) = 0$. Thus, in this case, the hot spots effectively decouple from the softest nematic fluctuations, similarly to what was obtained for an Ising-nematic tetragonal lattice [58]. On the other hand, if $\eta < 0$, the soft directions are $\zeta_{\mathbf{q}}^{(0)} = \theta, \theta \pm \pi/2$, implying that $|g(\mathbf{k}_{\text{hs}})| = |g_0|$, i.e. the hot spots are maximally coupled to the soft nematic fluctuations. For a generic non-circular Fermi surface respecting D_6 symmetry $g(\mathbf{k}_{\text{hs}})$ remains maximum for $\eta < 0$, but is expected to be non-zero albeit small for $\eta > 0$.

The sign of $\eta \equiv 1 - v_T^2/v_L^2$ is determined by the elastic action $S_{\text{el}}[\hat{\varepsilon}, \hat{\omega}]$. For a rigid crystal, $S_{\text{el}}[\hat{\varepsilon}, \hat{\omega}] = \frac{1}{2} \int_x [(\partial_\tau \mathbf{u})^2 + C_{ijkl} \varepsilon_{ij} \varepsilon_{kl}]$ depends only on the strain $\hat{\varepsilon}$, since global rotations do not cost energy. In a triangular lattice, there are only two independent elastic constants, $C_{11} \equiv C_{xxxx}$ and $C_{12} \equiv C_{xxyy}$, yielding $v_L^2 = C_{11}$ and $v_T^2 = (C_{11} - C_{12})/2$. Lattice stability requires $C_{11} > |C_{12}|$, which makes $\eta > 0$, implying that $g(\mathbf{k}_{\text{hs}})$ is small. However, the moiré superlattice is not

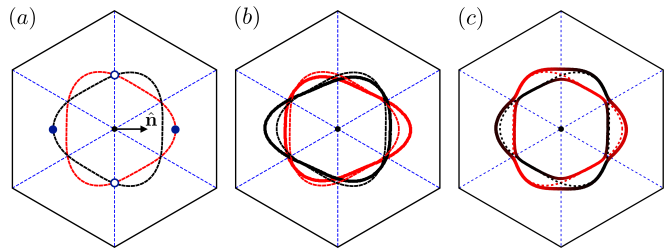


FIG. 4. (a) Fermi surface of the 6-band model of Ref. 65; red and black correspond to the two valleys. The two pairs of hot spots are marked by open and full symbols. (b) Distortion of the Fermi surface in the presence of intra-valley Potts-nematic order, with nematic director $\hat{\mathbf{n}}$ along the x axis. (c) Same as panel (b), but for inter-valley nematic order. In (b) and (c), the undistorted Fermi surface is shown by the dashed lines.

a rigid crystalline structure for small twist angles, as lattice relaxation leads to sharp domain walls separating the regions with AB and BA stacking. Because of this, arbitrary rotations of the moiré superlattice cost energy, and the elastic free energy acquires an extra term $\delta S_{\text{el}}[\hat{\omega}] = \frac{1}{2} \int_x K \omega_{xy}^2$ [50]. This term contributes only to the transverse velocity and when $K > 2(C_{11} + C_{12})$, v_T becomes larger than v_L (i.e. $\eta < 0$), implying that $|g(\mathbf{k}_{\text{hs}})|$ is maximum. Recent calculations of the acoustic phonon spectrum of TBG found that this condition is satisfied for small twist angles [49, 50], making TBG a rather unique system in which the Fermi-surface hot spots are maximally coupled to the nematic fluctuations.

To apply these results to TBG, we use the six-band model of Ref. 65. As shown in Fig. 4(a), there are two Fermi surfaces associated with the two valley degrees of freedom, and thus related by a C_{2z} rotation. Because the two pairs of hot spots for a given nematic director θ are related by $\pi/2$ rotations, they correspond to different valley symmetries. Setting $\theta = 0$ for concreteness, we find that the pair of hot spots located at $\theta_{\mathbf{k}_{\text{hs}}} = 0, \pi$ is associated with intra-valley nematicity [Fig. 4(b)], whereas the pair located at $\theta_{\mathbf{k}_{\text{hs}}} = \pm\pi/2$ is associated with inter-valley nematicity [Fig. 4(c)] (for details, see Supplementary Material).

We conclude by discussing the possible microscopic mechanisms for Potts-nematic order in TBG. In weak-coupling approaches, a Pomeranchuk-instability breaking the C_{3z} rotational-symmetry of the Fermi surface can be favored by van Hove singularities [66]. In strong-coupling approaches, where charge degrees of freedom are quenched, a widely used effective Hamiltonian is described in terms of an $SU(4)$ ‘‘super-spin’’ associated with spin and orbital variables [29, 40, 67–70]. Nematicity is then described by an ordering of the orbital variables, i.e. ordering in the $SU(2)$ orbital sector, which breaks spatial rotational symmetry. Whether the ground state of the effective $SU(4)$ Hamiltonian is a nematic phase is an interesting open question. A third possible mechanism is

a nematic phase that is a vestigial order of a primary electronic ordered state that breaks C_{3z} and some additional symmetry [39], such as $p + p$ -wave/ $d + d$ -wave superconductivity [40, 44, 52] or stripe spin density-waves [53].

Conclusions. We showed that the Potts-like character of the nematic order parameter in triangular moiré superlattices leads to unique nematic behaviors seen neither in tetragonal systems nor in rigid triangular crystals. Notably, a nematic-flop phase transition that spontaneously breaks the in-plane twofold rotational symmetries can still take place even when C_{3z} symmetry-breaking strain is applied. This makes it possible to unambiguously detect long-range nematic order in TBG despite the unavoidable presence of residual strains that break the same symmetry as the nematic order parameter. Moreover, the emergence of a nemato-orbital coupling mediated by acoustic phonons affects not only the character of the Potts-nematic transition, which becomes mean-field and first-order, but also the impact of the low-energy nematic fluctuations on the electronic properties, which is maximized due to the non-rigid nature of the moiré superlattice.

We thank A. Chubukov, L. Fu, P. Jarillo-Herrero, J. Kang, H. Ochoa, H. C. Po, J. Schmalian, T. Senthil, and O. Vafek for fruitful discussions. R.M.F. was supported by the U. S. Department of Energy, Office of Science, Basic Energy Sciences, under Award No. de-sc0020045.

-
- [1] Y. Cao, V. Fatemi, S. Fang, K. Watanabe, T. Taniguchi, E. Kaxiras, and P. Jarillo-Herrero, *Nature* **556**, 43 (2018).
- [2] Y. Cao, V. Fatemi, A. Demir, S. Fang, S. L. Tomarken, J. Y. Luo, J. D. Sanchez-Yamagishi, K. Watanabe, T. Taniguchi, E. Kaxiras, R. C. Ashoori, and P. Jarillo-Herrero, *Nature* **556**, 80 (2018).
- [3] M. Yankowitz, S. Chen, H. Polshyn, Y. Zhang, K. Watanabe, T. Taniguchi, D. Graf, A. F. Young, and C. R. Dean, *Science* **363**, 1059 (2019).
- [4] X. Lu, P. Stepanov, W. Yang, M. Xie, M. A. Aamir, I. Das, C. Urgell, K. Watanabe, T. Taniguchi, G. Zhang, A. Bachtold, A. H. MacDonald, and D. K. Efetov, *Nature* **574**, 653 (2019).
- [5] A. L. Sharpe, E. J. Fox, A. W. Barnard, J. Finney, K. Watanabe, T. Taniguchi, M. A. Kastner, and D. Goldhaber-Gordon, *Science* **365**, 605 (2019).
- [6] M. Serlin, C. Tschirhart, H. Polshyn, Y. Zhang, J. Zhu, K. Watanabe, T. Taniguchi, L. Balents, and A. Young, arXiv:1907.00261 (2019).
- [7] C. Shen, N. Li, S. Wang, Y. Zhao, J. Tang, J. Liu, J. Tian, Y. Chu, K. Watanabe, T. Taniguchi, R. Yang, Z. Y. Meng, D. Shi, and G. Zhang, arXiv:1903.06952 (2019).
- [8] X. Liu, Z. Hao, E. Khalaf, J. Y. Lee, K. Watanabe, T. Taniguchi, A. Vishwanath, and P. Kim, arXiv:1903.08130 (2019).
- [9] Y. Cao, D. Rodan-Legrain, O. Rubies-Bigordà, J. M. Park, K. Watanabe, T. Taniguchi, and P. Jarillo-Herrero, arXiv:1903.08596 (2019).
- [10] G. Chen, L. Jiang, S. Wu, B. Lyu, H. Li, B. L. Chittari, K. Watanabe, T. Taniguchi, Z. Shi, J. Jung, Y. Zhang, and F. Wang, *Nature Physics* **15**, 237 (2019).
- [11] G. Chen, A. L. Sharpe, P. Gallagher, I. T. Rosen, E. J. Fox, L. Jiang, B. Lyu, H. Li, K. Watanabe, T. Taniguchi, J. Jung, Z. Shi, D. Goldhaber-Gordon, Y. Zhang, and F. Wang, *Nature* **10** (2019).
- [12] J. M. B. L. dos Santos, N. M. R. Peres, and A. H. C. Neto, *Phys. Rev. Lett.* **99**, 256802 (2007).
- [13] R. Bistritzer and A. H. MacDonald, *Proceedings of the National Academy of Sciences* **108**, 12233 (2011).
- [14] E. J. Mele, *Phys. Rev. B* **84**, 235439 (2011).
- [15] J. M. B. L. dos Santos, N. M. R. Peres, and A. H. C. Neto, *Phys. Rev. B* **86**, 155449 (2012).
- [16] N. N. T. Nam and M. Koshino, *Phys. Rev. B* **96**, 075311 (2017).
- [17] N. F. Q. Yuan and L. Fu, *Phys. Rev. B* **98**, 045103 (2018).
- [18] H. C. Po, L. Zou, A. Vishwanath, and T. Senthil, *Phys. Rev. X* **8**, 031089 (2018).
- [19] M. Koshino, N. F. Q. Yuan, T. Koretsune, M. Ochi, K. Kuroki, and L. Fu, *Phys. Rev. X* **8**, 031087 (2018).
- [20] L. Zou, H. C. Po, A. Vishwanath, and T. Senthil, *Phys. Rev. B* **98**, 085435 (2018).
- [21] J. Kang and O. Vafek, *Physical Review X* **8**, 031088 (2018).
- [22] L. Rademaker and P. Mellado, *Phys. Rev. B* **98**, 235158 (2018).
- [23] Y.-H. Zhang, D. Mao, Y. Cao, P. Jarillo-Herrero, and T. Senthil, *Phys. Rev. B* **99**, 075127 (2019).
- [24] L. Zhang, *Science Bulletin* **64**, 495 (2019).
- [25] B. Lian, Z. Wang, and B. A. Bernevig, *Phys. Rev. Lett.* **122**, 257002 (2019).
- [26] F. Wu and S. Das Sarma, *Phys. Rev. B* **99**, 220507 (2019).
- [27] Y.-P. Lin and R. M. Nandkishore, *Phys. Rev. B* **100**, 085136 (2019).
- [28] Z. Song, Z. Wang, W. Shi, G. Li, C. Fang, and B. A. Bernevig, *Physical Review Letters* **123**, 036401 (2019).
- [29] J. Kang and O. Vafek, *Phys. Rev. Lett.* **122**, 246401 (2019).
- [30] G. Tarnopolsky, A. J. Kruchkov, and A. Vishwanath, *Phys. Rev. Lett.* **122**, 106405 (2019).
- [31] Y. Xie, B. Lian, B. Jäck, X. Liu, C.-L. Chiu, K. Watanabe, T. Taniguchi, B. A. Bernevig, and A. Yazdani, *Nature* **572**, 101 (2019).
- [32] Y. Choi, J. Kemmer, Y. Peng, A. Thomson, H. Arora, R. Polski, Y. Zhang, H. Ren, J. Alicea, G. Refael, F. v. Oppen, K. Watanabe, T. Taniguchi, and S. Nadj-Perge, *Nature Physics* **15**, 1174 (2019).
- [33] A. Kerelsky, L. J. McGilly, D. M. Kennes, L. Xian, M. Yankowitz, S. Chen, K. Watanabe, T. Taniguchi, J. Hone, C. Dean, A. Rubio, and A. N. Pasupathy, *Nature* **572**, 95 (2019).
- [34] Y. Jiang, X. Lai, K. Watanabe, T. Taniguchi, K. Haule, J. Mao, and E. Y. Andrei, *Nature* **573**, 91 (2019).
- [35] P. Jarillo-Herrero, KITP Workshop: Correlations in Moiré Flat Bands (2019).
- [36] Y.-H. Zhang, H. C. Po, and T. Senthil, arXiv:1904.10452 (2019).
- [37] S. Liu, E. Khalaf, J. Y. Lee, and A. Vishwanath, arXiv:1905.07409 (2019).
- [38] E. Fradkin, S. A. Kivelson, M. J. Lawler,

- J. P. Eisenstein, and A. P. Mackenzie, Annual Review of Condensed Matter Physics **1**, 153 (2010).
- [39] R. M. Fernandes, P. P. Orth, and J. Schmalian, Annual Review of Condensed Matter Physics **10**, 133 (2019).
- [40] J. W. F. Venderbos and R. M. Fernandes, Phys. Rev. B **98**, 245103 (2018).
- [41] J. F. Dodaro, S. A. Kivelson, Y. Schattner, X. Q. Sun, and C. Wang, Phys. Rev. B **98**, 075154 (2018).
- [42] H. Isobe, N. F. Q. Yuan, and L. Fu, Phys. Rev. X **8**, 041041 (2018).
- [43] V. Kozii, H. Isobe, J. W. F. Venderbos, and L. Fu, Phys. Rev. B **99**, 144507 (2019).
- [44] D. V. Chichinadze, L. Classen, and A. V. Chubukov, arXiv:1910.07379 (2019).
- [45] A. Uri, S. Grover, Y. Cao, J. Crosse, K. Bagani, D. Rodan-Legrain, Y. Myasoedov, K. Watanabe, T. Taniguchi, P. Moon, M. Koshino, P. Jarillo-Herrero, and E. Zeldov, arXiv:1908.04595 (2019).
- [46] T. Cea, N. R. Waler, and F. Guinea, arXiv:1906.10570 (2019).
- [47] J. H. Wilson, Y. Fu, S. Das Sarma, and J. H. Pixley, arXiv:1908.02753 (2019).
- [48] R. M. Fernandes, A. V. Chubukov, and J. Schmalian, Nature Physics **10**, 97 (2014).
- [49] M. Koshino and Y.-W. Son, Phys. Rev. B **100**, 075416 (2019).
- [50] H. Ochoa, Phys. Rev. B **100**, 155426 (2019).
- [51] The main results presented here also hold if one instead considers the approach in which TBG is described in terms of the D_3 point group.
- [52] M. Hecker and J. Schmalian, npj Quantum Materials **3**, 26 (2018).
- [53] A. Little, C. Lee, C. John, S. Doyle, E. Maniv, N. L. Nair, W. Chen, D. Rees, J. W. Venderbos, R. Fernandes, J. G. Analytis, and J. Orenstein, arXiv:1908.00657 (2019).
- [54] S. Jin, W. Zhang, X. Guo, X. Chen, X. Zhou, and X. Li, arXiv:1910.11880 (2019).
- [55] F. Y. Wu, Rev. Mod. Phys. **54**, 235 (1982).
- [56] D. Blankschtein and A. Aharony, Journal of Physics C: Solid State Physics **13**, 4635 (1980).
- [57] U. Karahasanovic and J. Schmalian, Phys. Rev. B **93**, 064520 (2016).
- [58] I. Paul and M. Garst, Phys. Rev. Lett. **118**, 227601 (2017).
- [59] V. de Carvalho and R. Fernandes, arXiv:1906.03205 (2019).
- [60] F. Wu, A. H. MacDonald, and I. Martin, Phys. Rev. Lett. **121**, 257001 (2018).
- [61] M. Angeli, E. Tosatti, and M. Fabrizio, arXiv preprint arXiv:1904.06301 (2019).
- [62] F. Wu, E. Hwang, and S. Das Sarma, Phys. Rev. B **99**, 165112 (2019).
- [63] R. A. Cowley, Phys. Rev. B **13**, 4877 (1976).
- [64] R. Folk, H. Iro, and F. Schwabl, Zeitschrift für Physik B Condensed Matter **25**, 69 (1976).
- [65] H. C. Po, L. Zou, T. Senthil, and A. Vishwanath, Phys. Rev. B **99**, 195455 (2019).
- [66] B. Valenzuela and M. A. H. Vozmediano, New Journal of Physics **10**, 113009 (2008).
- [67] C. Xu and L. Balents, Phys. Rev. Lett. **121**, 087001 (2018).
- [68] L. Classen, C. Honerkamp, and M. M. Scherer, Phys. Rev. B **99**, 195120 (2019).
- [69] D. Kiese, F. L. Buessen, C. Hickey, S. Trebst, and M. M. Scherer, arXiv:1907.09490 (2019).
- [70] W. Natori, R. Nutakki, R. Pereira, and E. Andrade, arXiv:1908.09224 (2019).

Supplementary material for “Nematicity with a twist: rotational symmetry breaking in a moiré superlattice”

SIX-BAND TIGHT-BINDING MODEL

Here we provide the details of implementing nematic order in the six-band tight-binding model for twisted bilayer graphene (TBG) introduced in Ref. 65. We will generally follow the notation and convention of Ref. 65, with the exception of a few minor modifications which simplify the notation for the present purposes.

The six-band tight-binding model of Ref. 65 is defined by (p_z, p_+, p_-) orbitals on the sites of a triangular lattice and s orbitals on the sites of a kagome lattice, as shown in Fig. S1. The purpose of the six-band model is to reproduce the low-energy flat bands of TBG in such a way that all symmetries manifestly present in the continuum description are respected (and are implemented naturally). The authors of Ref. 65 introduce a number of models which achieve this; here we choose the six-band model to study nematic order in TBG.

It is important to note that the six-band model describes the two low-energy flat bands originating from a *single* valley of the two graphene sheets forming the bilayer system. This implies that a model which includes the full set of flat low-energy bands (apart from spin) must have twelve bands: two copies of the six-band model related by the symmetries which exchange valleys. Here we sketch how such model is constructed and show how it can be supplemented with the appropriate symmetry breaking terms to account for nematic order.

We begin by recalling the definition of the six-band model. The orbital degrees of freedom can be represented by a fermion operator $\psi_{\mathbf{k}}^\dagger$ given by

$$\psi_{\mathbf{k}}^\dagger = (p_{\mathbf{k}z}^\dagger, p_{\mathbf{k}+}^\dagger, p_{\mathbf{k}-}^\dagger, a_{\mathbf{k}}^\dagger, b_{\mathbf{k}}^\dagger, c_{\mathbf{k}}^\dagger). \quad (\text{S1})$$

Note that this is a slight departure from Ref. 65. In terms of these degrees of freedom the (six-band) Hamiltonian for a single valley is given by [65]

$$H_{\mathbf{k}} = \begin{pmatrix} H_{p_z} + \mu_{p_z} & C_{p_{\pm}p_z}^\dagger & 0 \\ C_{p_{\pm}p_z} & H_{p_{\pm}} + \mu_{p_{\pm}} & C_{\kappa p_{\pm}}^\dagger \\ 0 & C_{\kappa p_{\pm}} & H_{\kappa} + \mu_{\kappa} \end{pmatrix}. \quad (\text{S2})$$

Here H_{p_z} and $H_{p_{\pm}}$ are the subblock Hamiltonians in the p_z and p_{\pm} subspaces, and H_{κ} describes the coupling between the kagome lattice sites. The subblocks C_{XY} describe the couplings between the X and Y sectors (where $X, Y = p_z, p_{\pm}, \kappa$). The form of all these subblocks are given in Ref. 65, including the parameter set we use here (see Table VI in Ref. 65).

To promote the six-band model to a full twelve-band model, we take two copies and introduce a valley degree of freedom as

$$\Psi_{\mathbf{k}}^\dagger = (\psi_{\mathbf{k}+}^\dagger, \psi_{\mathbf{k}-}^\dagger), \quad (\text{S3})$$

where \pm labels the K and K' valleys of the individual graphene layers. The full Hamiltonian $\mathcal{H}_{\mathbf{k}}$ is then given by

$$\mathcal{H}_{\mathbf{k}} = \begin{pmatrix} H_{\mathbf{k}} & \\ & U H_{-\mathbf{k}} U^\dagger \end{pmatrix}, \quad (\text{S4})$$

where $H_{\mathbf{k}}$ is the Hamiltonian of Eq. (S2) and $U \equiv U_{C_{2z}}$ is the matrix representation of the twofold rotation C_{2z} . A word of caution with respect to the tight-binding gauge choice is appropriate here. Ref. 65 uses a gauge for which $H_{\mathbf{k}+\mathbf{G}} = H_{\mathbf{k}}$ holds, where \mathbf{G} is a reciprocal lattice vector. In this gauge the matrix U is momentum dependent and thus takes a more complicated form. A simpler form is obtained in the more conventional tight-binding gauge, in which case matrix representations of symmetries are momentum independent. In particular, in the tight-binding gauge U is given by $U = \text{Diag}(1, -1, -1, 1, 1, 1)$. In what follows we will adhere to the gauge choice of Ref. 65.

The Hamiltonian of Eq. (S4) with the parameters specified in Ref. 65 defines a tight-binding model for TBG that respects all symmetries, including a $U_v(1)$ valley conservation symmetry. Various symmetry breaking terms can be considered, and here we are specifically interested in terms that break C_{3z} symmetry but preserve C_{2z} symmetry, as required by quadrupolar nematic order. The $U_v(1)$ valley symmetry is not directly relevant to Potts-nematic order, but it is nonetheless an important property of the TBG system and therefore it is useful to specify whether or not it is preserved by additional symmetry breaking terms.

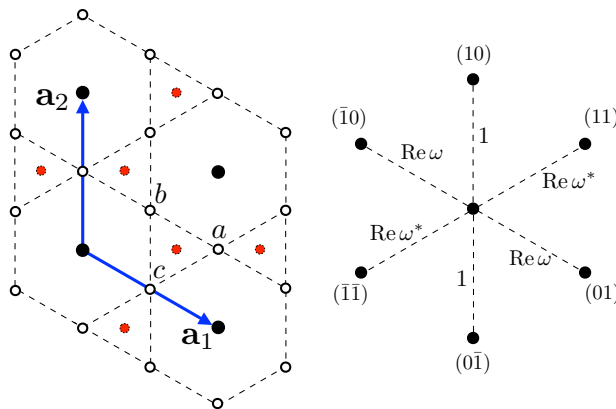


FIG. S1. The model of Ref. 65 is defined by (p_z, p_+, p_-) orbitals on sites of a triangular lattice (indicated by black solid dots) and s orbitals on the sites of a kagome lattice (indicated by solid white dots). Note that the kagome lattice sites are located on the edges of the triangular Wigner-Seitz cell. The Bravais lattice vectors $\mathbf{a}_{1,2}$ used in Eq. (S8) are shown in blue. The three kagome sites in the unit cell are labeled (a, b, c) . The position of the honeycomb lattice sites are indicated by red dots, but do not play a role in our analysis.

Let us first note that a coupling of the valleys of the form

$$\delta\mathcal{H} = \Delta \sum_{\mathbf{k}} \psi_{\mathbf{k}+}^\dagger \psi_{\mathbf{k}-} + \text{H.c.}, \quad (\text{S5})$$

breaks the $U_v(1)$ valley but respects all lattice symmetries as well as time-reversal symmetry. Added to the Hamiltonian of Eq. (S4) it enters as an off-diagonal block. The Fermi surfaces of the Hamiltonian in the absence and presence of Eq. (S5) are shown in Figs. S2(a) and (b), respectively.

ROTATIONAL SYMMETRY BREAKING

Next, we consider the rotational symmetry breaking terms that constitute nematic order. Since the model is built from multiple degrees of freedom, there are a number of different ways in which rotation symmetry breaking can be implemented. We first focus on the triangular lattice sector of the model. Within this sector there are two possibilities: nematic order can occur as a result of hopping anisotropy or due to a lifting of the orbital degeneracy. To model the first possibility we introduce the two d -wave form factors

$$d_{\mathbf{k}1} = \phi_{01} + \text{Re } \omega^* \phi_{\bar{1}\bar{1}} + \text{Re } \omega \phi_{10} + \text{c.c.} \quad (\text{S6})$$

$$d_{\mathbf{k}2} = \text{Im } \omega^* \phi_{\bar{1}\bar{1}} + \text{Im } \omega \phi_{10} + \text{c.c.}, \quad (\text{S7})$$

where the phases ϕ_{lm} are defined as (see Ref. 65)

$$\phi_{lm} = e^{-i\mathbf{k} \cdot (l\mathbf{a}_1 + m\mathbf{a}_2)}. \quad (\text{S8})$$

Here we use the notation $\bar{l} \equiv -l$ and $\omega = \exp(2\pi i/3)$. The hopping pattern of the d -wave form factor $d_{\mathbf{k}1}$ is graphically shown in Fig. S1. These form factors have precisely the same symmetry as (Φ_1, Φ_2) introduced in the main text.

The triangular lattice d -wave form factors can then be used to introduce a symmetry breaking perturbation in the triangular lattice (p -orbital) sector. For instance, we can add a perturbation δH_{p_z} to the Hamiltonian H_{p_z} of the p_z orbital appearing in Eq. (S2) given by

$$\delta H_{p_z} = \Phi_1 d_{\mathbf{k}1} + \Phi_2 d_{\mathbf{k}2}, \quad (\text{S9})$$

where $\Phi_{1,2}$ are the nematic order parameters as defined in the main text. This term gives the Fermi surface distortion of Fig. 4(b) of the main text. Clearly, the same perturbation (but proportional to the appropriate identity matrix) can be added to H_{p_\pm} , which describes the p_\pm orbitals.

In the p_\pm -orbital sector the nematic order parameter couples to another symmetry breaking perturbation, which is independent of momentum. Making the two orbitals inequivalent lifts their degeneracy and necessarily breaks

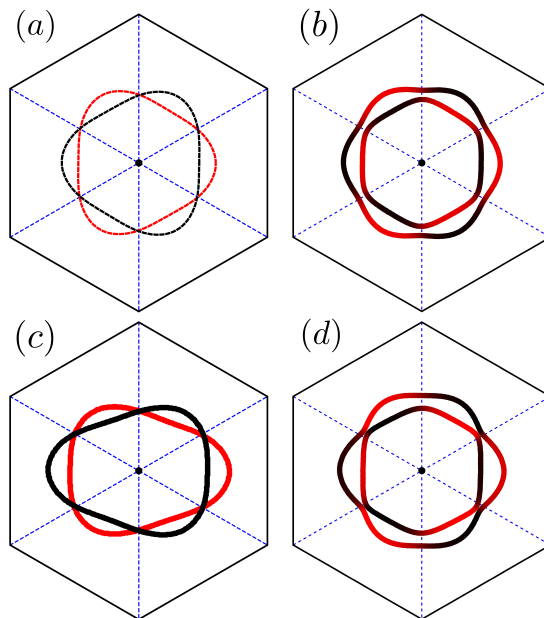


FIG. S2. Fermi surface of the 6-band model of Ref. 65 with parameters as specified in Ref. 65 ; red and black correspond to the two valleys of the individual graphene sheets (reproduced from the main text). (b) Fermi surface of the same model as in (a) but with the additional $U_v(1)$ valley symmetry breaking terms given by Eq. (S5). Colors (black and red) correspond to the projection of eigenstates on the two valleys. (c) Fermi surface in the presence of (intra-valley) orbital nematic order given by Eq. (S10). (d) Fermi surface in the presence of *inter*-valley nematic order given by Eq. (S14).

threefold rotation symmetry. In particular, the perturbation $\delta H_{p\pm}$ which achieves this is given by

$$\delta H_{p\pm} = \begin{pmatrix} 0 & \Phi_1 - i\Phi_2 \\ \Phi_1 + i\Phi_2 & 0 \end{pmatrix}. \quad (\text{S10})$$

Note that the diagonal terms are zero since time-reversal symmetry must be preserved. (An overall energy can be absorbed in $\mu_{p\pm}$.) The Fermi surface in the presence of a nematic distortion given by $\delta H_{p\pm}$ is shown in Fig. S2(c). As argued and expected, the distortion is qualitatively similar to a distortion originating from *d*-wave form factors in the kinetic terms (Fig. 4(b) of the main text).

In Fig. S3, we show the change in the Fermi momentum due to nematic order, δk_F , corresponding to the Fermi surface of Fig. 4(b) of the main text. Blue and yellow denote positive and negative values, respectively. First, we see that the shape of δk_F corresponds to what one expects from the *d*-wave form factor in hexagonal lattices. Second, we note that the maximum δk_F occurs precisely at the hot spot identified in Fig. 4(a) of the main text.

Consider next the kagome lattice sector of the model. The kagome sector does not have an orbital degree of freedom but it does have multiple sites in the unit cell. The simplest coupling to the nematic order parameter is given by a charge ordering perturbation within the unit cell, which breaks threefold rotations but preserves the twofold rotation C_{2z} . Specifically, the perturbation δH_κ to the kagome lattice Hamiltonian H_κ is given by

$$\delta H_\kappa = (\Phi_1 - i\Phi_2) \begin{pmatrix} 1 & \\ & \omega \\ & & \omega^* \end{pmatrix} + \text{H.c.}, \quad (\text{S11})$$

The rotational symmetry breaking perturbations introduced so far are all intra-valley perturbations; they should be considered as perturbations to Eq. (S2), with the full Hamiltonian given by the prescription of Eq. (S4). One may, however, also consider inter-valley nematic coupling terms, which enter the off-diagonal blocks in Eq. (S4). More precisely, the Hamiltonian of Eq. (S4) is modified according to

$$\mathcal{H}_\mathbf{k} \rightarrow \begin{pmatrix} H_\mathbf{k} & \\ & UH_{-\mathbf{k}}U^\dagger \end{pmatrix} + \delta\mathcal{H}_\Phi, \quad (\text{S12})$$

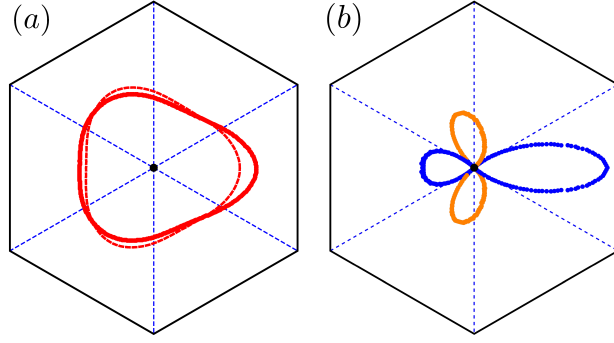


FIG. S3. To demonstrate the d -wave symmetry of the Fermi surface distortion in the presence of intra-valley nematic order we show δk_F , i.e. the change in Fermi momentum, as function of angle. Panel (a) shows the (single-valley) distorted Fermi surface of Fig. 4(b) of the main text and panel (b) shows δk_F , which clearly exhibits four nodes and a sign change (indicated by different colors) at the nodes.

where $\delta\mathcal{H}_\Phi$ collects all terms which describe nematic distortions and takes the form

$$\delta\mathcal{H}_\Phi = \begin{pmatrix} & \Delta_\Phi \\ \Delta_\Phi^\dagger & \end{pmatrix}. \quad (\text{S13})$$

The form of Δ_Φ depends on the choice of nematic coupling; as in the case of intra-valley nematic coupling, in principle many possibilities of inter-valley nematic coupling exist. One simple type of nematic coupling is given by

$$\Delta_\Phi = \delta H_{p_z} \oplus \delta H_{p_\pm}, \quad (\text{S14})$$

where δH_{p_z} and δH_{p_\pm} are given by Eqs. (S9) and (S10). The Fermi surface corresponding to inter-valley nematic coupling of this form is shown in Fig. S2(d).

We have based our microscopic discussion of rotation symmetry breaking on the model introduced in Ref. 65. This was motivated by the natural implementation of all relevant symmetries in this model. It is worth stressing that an analysis of nematic order in TBG similar to the one presented here can also be obtained from different microscopic (tight-binding) models proposed for TBG [17–20, 29].
